Noname manuscript No.
(will be inserted by the editor)

The Q^p_{Weak} Experiment

A Search For Physics Beyond The Standard Model Via A Measurement Of The Proton's Weak Charge

D. Androic[a], D.S. Armstrong[b], A. Asaturyan[o], T. Averett[b], J. Balewski[s], J. Beaufait[d], R.S. Beminiwattha[c], J. Benesch[d], F. Benmokhtar[e], J. Birchall[f], R.D. Carlini[d,b], J.C. Cornejo[b], S. Covrig[d], M.M. Dalton[g], C.A. Davis[m], W. Deconinck[b], J. Diefenbach[q], K. Dow[s], J.F. Dowd[b], J.A. Dunne[l], D. Dutta[l], W.S. Duvall[k], M. Elaasar[t], W.R. Falk[f], J.M. Finn[b]*, T. Forest[u], D. Gaskell[d], M.T.W. Gericke[f], J. Grames[d], V.M. Gray[b], K. Grimm[b], F. Guo[s], J.R. Hoskins[b], K. Johnston[p], D. Jones[g], M. Jones[d], R. Jones[v], M. Kargiantoulakis[g], P.M. King[c], E. Korkmaz[j], S. Kowalski[s], J. Leacock[k], J. Leckey[b], A.R. Lee[k], J.H. Lee[b,c], L. Lee[f], S. MacEwan[f], D. Mack[d], J.A. Magee[b], R. Mahurin[f,d], J. Mammei[f], J. Martin[r], M. McHugh[i], D. Meekins[d], J. Mei[d], R. Michaels[d], A. Micherdzinska[i], K.E. Myers[i], A. Mkrtchyan[o], H. Mkrtchyan[o], A. Narayan[l], L.Z. Ndukum[l], V. Nelyubin[g], Nuruzzaman[q], W.T.H van Oers[f,m], A.K. Opper[i], S.A. Page[f], J. Pan[f], K. Paschke[g], S.K. Phillips[n], M.L. Pitt[k], M. Poelker[d], J.F. Rajotte[s], W.D. Ramsay[f,m], J. Roche[c], B. Sawatzky[d], T. Seva[a], M.H. Shabestari[l], R. Silwal[g], N. Simicevic[p], G. Smith[d], P. Solvignon[d], D.T. Spayde[h], A. Subedi[l], R. Subedi[i], R. Suleiman[d], V. Tadevosyan[o], W.A. Tobias[g], V. Tvaskis[f], B. Waidyawansa[c], P. Wang[f], S.P. Wells[p], S.A. Wood[d], S. Yang[b], R.D. Young[w], S. Zhamkochyan[o], D. Zou[s]

Received: date / Accepted: date

Abstract In May 2012, the Q^p_{Weak} collaboration completed a two year measurement program to determine the weak charge of the proton $Q^p_W = \left(1 - 4\sin^2\theta_W\right)$ at the Thomas Jefferson National Accelerator Facility (TJNAF). The experiment was designed to produce a 4.0% measurement of the weak charge, via a 2.5% measurement of the parity violating asymmetry in the number of elastically scattered 1.165 GeV electrons from protons, at forward angles. At the proposed precision, the experiment would produce a 0.3% measurement of the weak mixing angle at a momentum transfer of $Q^2 = 0.026$ GeV^2, making it the most precise stand alone measurement of the weak mixing angle at low momentum transfer. In combination with other parity measurements, Q^p_{Weak} will also provide a high precision determi-

[a]University of Zagreb

[b]The College of William and Mary

[o]Yerevan Physics Institute

[s]Massachusetts Institute of Technology

[d]Thomas Jefferson National Accelerator Facility

[c]Ohio University

[e]Duquesne University

[f]University of Manitoba

[g]University of Virginia

[m]TRIUMF

[q] Hampton University

[l]Mississippi State University

[k]Virginia Polytechnic Institute and State University

[t]Southern University at New Orleans

*deceased

[u]Idaho State University

[p]Louisiana Tech University

[v]University of Connecticut

[j]University of Northern British Columbia

[r]University of Winnipeg

[i]George Washington University

[n]University of New Hampshire

[h]Hendrix College

[w]University of Adelaide

M.T.W. Gericke
University of Manitoba
Tel.: +204-474-6203
Fax: +204-474-7622
E-mail: mgericke@physics.umanitoba.ca

nation of the weak charges of the up and down quarks. At the proposed precision, a significant deviation from the Standard Model prediction could be a signal of new physics at mass scales up to $\simeq 6$ TeV, whereas agreement would place new and significant constraints on possible Standard Model extensions at mass scales up to $\simeq 2$ TeV. This paper provides an overview of the physics and the experiment, as well as a brief look at some preliminary diagnostic and analysis data.

Keywords Standard Model · Weak Charge · Parity Violation · Electron Scattering · New Physics

PACS 12.15.Mm · 12.60.Cn · 25.30.Bf · 11.30.Er

1 Introduction

Precision measurements at moderate and low energies can provide important information in the search for physics beyond the Standard Model (SM), in a way that is complementary to direct new particle searches at high energy colliders, such as the Large Hadron Collider (LHC) at CERN. For instance, while the LHC may discover a new heavy boson, it may not necessarily be able to identify its role or how it couples to the particles of the SM. Such questions can sometimes be answered by other experiments that look for a discrepancy of suppressed and sensitive observables with their SM predicted values [1,2]. The significance of low energy searches becomes even more evident when one compares several experiments with differing dependencies on a particular model. A case in point would be the measurements of the proton and electron [3] weak charges, which must both have a pull to larger values for Super-Symmetry (SUSY) loops, a pull in opposite directions (larger and smaller respectively) for R-parity violating SUSY, and a positive pull (no pull) for the proton weak charge (electron weak charge), for models involving leptoquarks.

The subject of this paper is the Q^p_{Weak} experiment, which completed a two year long measurement program in May 2012, in Hall C at the Thomas Jefferson National Accelerator Facility (TJNAF), to measure the weak charge of the proton $Q^p_W = 1 - 4\sin^2\theta_W \simeq 0.075$. The weak charge of the proton is a suppressed quantity in the SM and results from this experiment, in conjunction with previous and future measurements of parity-violating electron scattering, will therefore constrain the possibility of relevant physics beyond the Standard Model to the multi-TeV energy scale. The Q^p_{Weak} experiment started data production in fall 2010.

The experimental observable is the parity violating asymmetry in the number of elastically scattered electrons ($E_{beam} = 1.165$ GeV) from protons at very forward angles ($\theta = 8 \pm 2^\circ$). The aim is a measurement of the asymmetry with a $\pm 2.1\%$ statistical and $\pm 1.3\%$ systematic uncertainty. In terms of the weak charges and nucleon form factors, the asymmetry is given by [4][1]

$$A_{PV}(\mathbf{e}, p) = k(Q^2 Q^p_W + A_{H,V} + A_{H,A})$$

[1] $k \equiv -\frac{G_F}{4\pi\alpha\sqrt{2}}$, $\epsilon \equiv \frac{1}{1+2(1+\tau)\tan^2\frac{\theta}{2}}$, $\epsilon' \equiv \sqrt{\tau(1+\tau)(1-\epsilon^2)}$, and $\tau \equiv Q^2/4M_N^2$.

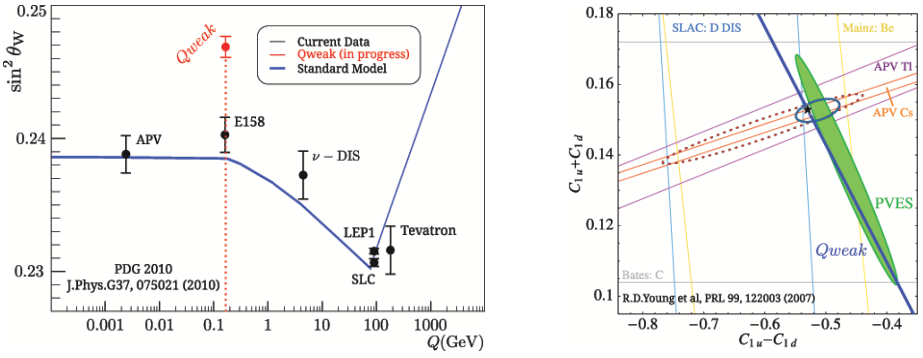

Fig. 1 Left: Calculated running of the weak mixing angle in the Standard Model, as defined in the modified minimal subtraction scheme [13]. The black error bars show completed measurements [14–17], while the red error bar (with arbitrarily chosen vertical location) refers to the proposed 4% Q^p_{Weak} measurement. Right: Constraints on the neutral weak effective couplings to up and down quarks [6]. The dotted contour displays the experimental limits (95% CL) reported in the PDG [17] together with the prediction of the Standard Model (black star). The solid blue line indicates the anticipated constraint from the planned Q^p_W measurement, assuming the SM value.

$$A_{H,V} = Q^n_W \frac{\epsilon G^{p,\gamma}_E G^{n,\gamma}_E + \tau G^{p,\gamma}_M G^{n,\gamma}_M}{\epsilon \left(G^{p,\gamma}_E\right)^2 + \tau \left(G^{p,\gamma}_M\right)^2} + Q^s_W \frac{\epsilon G^{p,\gamma}_E G^{s}_E + \tau G^{p,\gamma}_M G^{s}_M}{\epsilon \left(G^{p,\gamma}_E\right)^2 + \tau \left(G^{p,\gamma}_M\right)^2}$$

$$A_{H,A} = Q^e_W \frac{\epsilon' G^{p,Z}_A G^{p,\gamma}_M}{\epsilon \left(G^{p,\gamma}_E\right)^2 + \tau \left(G^{p,\gamma}_M\right)^2} \ . \tag{1}$$

At the chosen momentum transfer ($Q^2 = 0.026$ GeV^2), the SM predicted size of the asymmetry is $\simeq -230$ ppb. Based on this prediction, the goal uncertainty is $\simeq \pm 6$ ppb. Besides the proton weak charge, the asymmetry has contributions from hadronic form factors. At tree level, the first term in the asymmetry is proportional to the weak charge of the proton $Q^p_W = \left(1 - 4\sin^2\theta_W\right)$ and has a Standard Model predicted value of $\simeq -150$ ppb. This term has contributions from radiative corrections, as well as from possible new physics. The hadronic portion of the asymmetry has two terms, corresponding to the vector and axial vector hadronic currents. These are parameterized in terms of the electromagnetic form factors of the neutron and proton ($G^{p,\gamma}_E$, $G^{n,\gamma}_E$, $G^{p,\gamma}_M$, $G^{n,\gamma}_M$), as well as the strange and axial form factors (G^s_E, G^s_M, $G^{p,Z}_A$) respectively. At the chosen kinematics, the vector contribution to the asymmetry is about $\simeq -70$ ppb, while the axial vector contribution is about $\simeq -10$ ppb. The asymmetry decreases with momentum transfer, making the measurement at lower Q^2 harder. However, at this low Q^2, the weak charge contribution to the asymmetry has been maximized relative to the contributions from hadronic effects, while still allowing the measurement of the asymmetry within a reasonable time. This is possible, because the hadronic terms have an overall Q^4 dependence, while the weak charge term has a Q^2 dependence. The hadronic contributions are well constrained by the world data set [5,6].

The SM and extensive calculations of radiative corrections [7–12] allow for a precise prediction of Q^p_W, as a function of the weak mixing angle, $\sin^2\theta_W$, from the Z^0 pole down to low energies, as shown in Fig. 1. The precise measurements

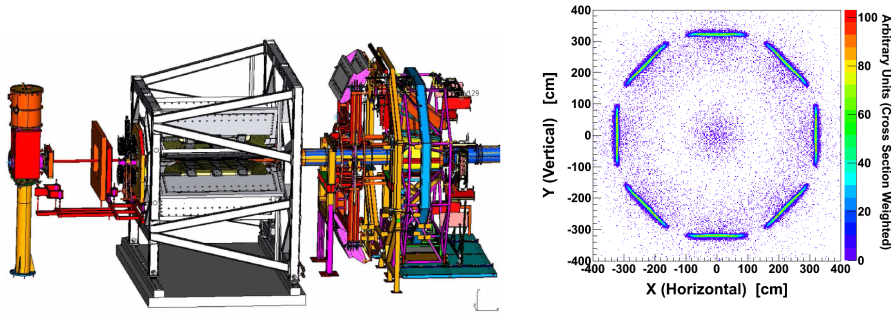

Fig. 2 Left: Engineering drawing of the experimental layout. The beam runs from left to right in the figure. Right: Simulated event pattern in the focal plane for all eight octants. Only elastic events are shown.

near the Z^0 pole anchor the curve at one particular energy scale. The shape of the curve away from this point is a prediction of the SM and to test this prediction one needs precise, off-peak measurements.

Beyond tree level, the weak charge of the proton can be written as $Q^p_W = \rho_{PV}\left(1 - 4\kappa_{PV}\sin^2\theta_W\right) + \lambda_p = -2\left(2C_{1u} + C_{1d}\right)$, where ρ_{PV}, κ_{PV}, and λ_p are parameters that contain both radiative corrections within the Standard Model, as well as contributions from possible new physics [9]. The Standard Model radiative corrections for Q^p_W include terms from γZ, ZZ, WW box and other loop diagrams. Additional radiative corrections associated with fermion and massive vector boson loops collectively give rise to the scale dependence (running) of the weak mixing angle, as seen in Fig 1. The quark weak charges relevant for the Q^P_{Weak} experiment are $C_{1u} = \frac{1}{2}\rho'_{eq}\left(1 - \frac{8}{3}\kappa'_{eq}\sin^2\theta_W\right) + \lambda_{1u}$ and $C_{1d} = \frac{1}{2}\rho'_{eq}\left(-1 + \frac{4}{3}\kappa'_{eq}\sin^2\theta_W\right) + \lambda_{1d}$. Figure 1 shows the constraints on the quark weak charges, placed by the indicated completed measurements (From [6]). Combining the projected Q^p_W measurement (in blue) with the previous experimental results will therefore lead to a significant improvement in the allowed range of values for C_{1u} and C_{1d}. Assuming the Standard Model holds, the resulting new limits will significantly constrain new physics to be above a mass scale of ≈ 2 TeV, for new weakly coupled physics.

2 Experimental Overview

The experimental layout is shown in Fig. 2. The main challenges for this experiment arise from the small expected asymmetry (-230 ppb) and the high precision goal in connection with possible backgrounds and systematic effects. The experiment itself consists of well established technology. However, due to the high precision goal, several techniques were pushed to levels beyond where any other experiment has performed to date, both in precision and capacity. Examples of this include the target, which is the world's highest power liquid hydrogen (LH_2) target used in an electron scattering experiment [18], a very fast electron beam helicity reversal rate of 960 Hz (see below), and a very high electron polarization of 89%. See [19] for a full description of the experiment.

The measured or raw asymmetry for a given detector PMT is given by the following expressions:

$$A_{raw} = \frac{Y^+ - Y^-}{Y^+ + Y^-} = P\left(f_p A_{PV}(\mathbf{e}, p) + \sum_b f_b A_b\right) + A_{beam} + A_\epsilon \qquad (2)$$

$$Y^\pm = Y^o\left(1 \pm A_{raw}\right) \pm \epsilon\ . \qquad (3)$$

Here, $Y^\pm$ is the total signal yield seen in a given PMT for a right-handed (+) or left-handed (-) electron beam helicity state.The factors $f_p = \frac{\langle Y_p \rangle}{\langle Y \rangle}$ and $f_b = \frac{\langle Y_b \rangle}{\langle Y \rangle}$ are the fractional physics of interest and background contributions, respectively, to the total yield for the PMT. P is the beam polarization, the A_b are various background asymmetries, and $A_{beam} = A_{beam}(E, x, y, x', y')$ is the false asymmetry due to helicity correlated beam changes. The latter includes yield changes due to beam position (x, y), beam angle (x', y'), and beam energy (E) on target. The total yield is normalized to the beam current. The A_ϵ and ϵ terms are electronic contributions from a small (but possible) helicity signal leakage into the data acquisition (DAQ) electronics or the detector pedestal. With this in mind, the experiment was designed to make high precision measurements of the beam polarization, the momentum transfer, and the signal yield. The experiment was also designed to suppress backgrounds and helicity correlated electronic and beam effects as much as possible, and experimental components were included in the design, to allow ancillary measurements of both background asymmetries and yields, as well as helicity correlated beam parameter changes.

The experiment made use of two polarimeters, a Compton polarimeter, used for continuous polarization measurements at full current, and a Møller polarimeter used for short invasive polarimetry two or three times a week at lower currents. Measurement of beam parameters was facilitated by a series of beam current monitors, beam position monitors, luminosity monitors, and beam halo monitors. The polarimeters and beam monitors are located upstream of the target and are not shown in Fig. 2. From left to right in Fig. 2, a 180 μA 85% longitudinally polarized beam of 1.165 GeV electrons is incident on a LH_2 target with 2.5 kW of cooling power. The high power, low noise target provides the high luminosity needed to reach the statistical goal within the scheduled running time. The scattered electrons are collimated to define an average scattering angle of $\theta = 8 \pm 2^\circ$ and an azimuthal acceptance of 53% of 2π. The collimators were carefully designed and constructed to produce a well known Q^2 range and suppress backgrounds. An eight sector toroidal magnet focuses the scattered electrons onto a set of eight, two meter long quartz Čerenkov bars. The scattered beam profile is shown on the right-hand side in Fig. 2.

The octagonal symmetry arrangement of the detectors allows for various choices of detector combinations that suppress helicity correlated beam motion effects when extracting the asymmetry from the signal. The detectors are surrounded by heavy shielding walls and ceiling, to suppress ambient soft photon and neutron background present in the experimental hall. Four sets of wire chambers are used (two horizontal wire chambers (HDCs) before the magnet, at the collimators, and two vertical wire chambers (VDCs) in front of the detectors) to allow for calibration mode (at nA level beam currents) Q^2 determination and background measurements. The chambers are mounted on rotators, which allows measurements in

all 8 octants. For the Q^2 determination, the chambers provide two independent measurements of the electron tracks (before and after the spectrometer), which are connected in the analysis, using the accurately mapped spectrometer field. The HDCs are also used to determine the scattering vertex in the target. A single 1 cm^3 scanning Čerenkov detector is placed in front of one of the main Čerenkov detectors, to facilitate the Q^2 measurement at full beam current. Luminosity monitors are placed downstream of the main detectors.

At full current, the event rate per main detector is about 900 MHz and they are therefore operated in current mode. The size of the main detectors (2 meters long, 18 cm wide and 1.25 cm thick), their position ($\approx$ 3.8 meter radial distance from the forward beam line and $\approx$ 5.6 meters from the center of the magnet), and their angle with respect to the vertical (0°) were carefully chosen to maximize the elastic electron rate, maximize light output, and minimize backgrounds. The Čerenkov light is detected by two photomultiplier tubes (PMT) for each quartz bar; one on each side. A 2 cm thick lead pre-radiator is mounted in front of each quartz bar, to increase the light yield from scattered electrons, using showering, and to decrease the signal from photon backgrounds. The pre-radiated quartz detectors and the two PMTs together produce a light yield of about 90 photoelectrons per scattered electron event.

The experimental asymmetry must be corrected for backgrounds from electrons scattering off of the aluminum target windows, for backgrounds from inelastically scattered electrons as well as for soft photon and neutron background. Careful measurements of these backgrounds were done either through ancillary data runs, at various spectrometer field settings and beam energies, or in-situ, using background detectors placed in various locations around the main detectors.

3 Analysis and Some Preliminary Data

The data analysis for the asymmetry, polarization, and Q^2 measurements is ongoing. All results presented in this paper are preliminary and blinded (see below). Here we only present some diagnostic data and a small, blinded excerpt of asymmetry data for illustrative purposes. The primary technology used in the clean extraction of the asymmetry in Eqn. 2 is fast helicity reversal. Since any part of the signal seen in the detectors can and does fluctuate, the faster the helicity reversal, the more accurate is the description of the experimental apparatus as a linear measurement device. Possible signal changes include slow gain drifts, target density fluctuations, and beam drifts. The TJNAF laser source can accommodate high helicity reversal rates with high polarization, using a Pockels cell. Q^P_{Weak} routinely ran at a 960 Hz helicity reversal rate, coupled with a reversal pattern of $(+--+)$ or $(-++-)$ for consecutive helicity windows and with the initial window polarity changed pseudo-randomly. Either of these patterns removes any linear drift in the signal and the fast reversal makes the approximation of relatively slow random fluctuations as linear drifts valid. Experimental drifts and fluctuations, such as those mentioned above were measured during the experiment and verified to be slow compared with the helicity reversal.

The signal within each helicity window is integrated and a separate asymmetry is calculated for each helicity pattern, from Eqn. 2. When averaged over long time periods (in the Q^P_{Weak} case at least 5 minutes for a so called runlet, defined based

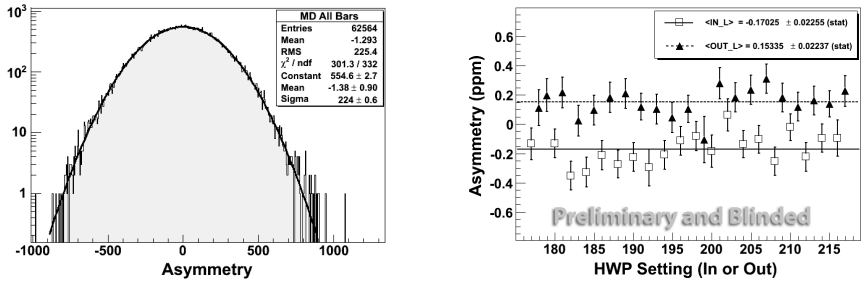

Fig. 3 Left: Histogram of pattern asymmetries with an RMS width that is slightly better than the expected width of $\simeq$ 230 ppm. Right: Asymmetries for different half-wave plate (HWP) settings (in and out), but for the same Wien setting (see definition in the text). The average size of the asymmetry is consistent with a simple sign change for the two HWP settings, within the statistical error. The asymmetries are preliminary and blinded with a 60 ppb box (see text). Each HWP setting consists of about 4 hours of data.

on a manageable file size), the small remaining asymmetries due to non-linear drifts should have random signs and average out. The only remnant of these drifts and fluctuations is then an increase in the measured root-mean-square (RMS) width of the distribution of measured asymmetries; a contribution to the statistical uncertainty above simple counting statistics. The proximity (or lack thereof) to the counting statistics RMS width is a measure of the efficiency and health of the experiment. A typical example of the asymmetry distribution is shown on the left in Fig. 3. The expected RMS width is $\simeq$ 230 ppm, including all contributions from counting statistics ($\simeq$ 200 ppm), detector resolution ($\simeq$ 90 ppm), beam current monitor resolution ($\simeq$ 50 ppm), and target boiling noise ($\simeq$ 60 ppm). An example of a measured RMS width of ($\simeq$ 225 ppm) is shown on the left in Fig. 3.

All remaining asymmetries are true systematic effects, such as those associated with helicity correlated beam changes and background physics. Sensitivities of the detectors to helicity correlated beam properties are measured in dedicated beam modulation runs, as well as from natural beam motion, during routine data production. These sensitivities are then used in regression, when the actual physics asymmetry of interest is extracted from the data. Additional helicity reversal techniques, so called slow reversal, are used to cancel systematic effects introduced in the source (e.g. at the photo cathode or in the Pockels cell). These include insertion of one or two half-wave plates after the Pockels cell, approximately every four hours, and a Wien electron spin rotation in the injector beam every few weeks. When a half-wave plate is inserted or a Wien flip is performed, the polarity (sign) of the asymmetry changes and the consistency with which this happens, without any changes in the size of the asymmetry, is an important measure of the systematic integrity of the experimental data. An example of this is shown on the right in Fig. 3. For the blinding, the raw asymmetries as defined in Eqn. 2, are shifted by an additive "blinding offset", which has a constant magnitude but changes sign with insertion and removal of the half-wave plate, or with a change of the Wien setting. The magnitude of the blinding offset is not known to the experimenters, but is calculated in the analysis software using a seeded random algorithm to select an offset value in the range of $\pm$60 ppb.

4 Conclusion

The Q^p_{Weak} collaboration has successfully completed a two year long measurement program with very high statistics and excellent control of systematic effects. This constitutes the first measurement of the proton weak charge and a search for new physics beyond the Standard Model up to mass scales of $\simeq$ 6 TeV (model dependent). The collaboration is currently working on the completion of the data analysis.

Acknowledgements We would like to extend a special thank you to Ernie Ihloff, Stan Sobczynski, Jason Bessuille and James Kelsey from MIT, John Hansknecht, Trent Allison and John Musson from Jefferson Laboratory, as well as George Clark and Bill Roberts from TRIUMF, for their important engineering support. This research was funded by the US Department of Energy (DOE),the US National Science Foundation (NSF), the Natural Sciences and Engineering Research Council of Canada (NSERC) and the Canadian Foundation for Innovation (CFI).

References

1. J. Erler and M. J. Ramsey-Musolf. *Prog. Part. Nucl. Phys.*, **54** 351–442, (2005).
2. M. J. Ramsey-Musolf and S. Su. hep-ph/0612057 (2006).
3. J. Mammei, In the proceedings of the PAVI11 conference, From Parity Violation to Hadronic Structure and more, *IL NUOVO CIMENTO*, **10.1393/ncc/i2012-11284-7**, (2012)
4. M. J. Musolf et al., *Phys. Rep.* **239**, 1 (1994).
5. J. Roche, R. D. Carlini, R.D. Young, and A.W. Thomas, *Phys. Rev. Lett.*, **97**:102002, (2006).
6. R. D. Carlini, A.W. Thomas, R.D. Young, and J. Roche, *Phys. Rev. Lett.*, **99**:122003, (2007).
7. P. G. Blunden, W. Melnitchouk, and A.W. Thomas, *Phys. Rev. Lett.* **107**:081801, (2011).
8. A. Sibirtsev, P. G. Blunden, W. Melnitchouk, and A.W. Thomas *Phys. Rev. D* **82**:013011, (2010).
9. A. Kurylov, M.J. Musolf, S. Su *Phys. Rev. D* **68**, 035008, (2003).
10. W. J. Marciano and A. Sirlin *Phys. Rev. D* **29**:75, (1984).
11. M. Gorchtein, C. J. Horowitz, and Michael J. Ramsey-Musolf *Phys. Rev. C* **84**:015502, (2011).
12. B. C. Rislow and C. E. Carlson *Phys. Rev. D* **83**:113007, (2011).
13. J. Erler and M. J. Ramsey-Musolf. *Phys. Rev.*, **D72**:073003, (2005).
14. S. C. Bennett and C. E. Wieman. *Phys. Rev. Lett.*, **82**:2484-2487, (1999).
15. P. L. Anthony et al. *Phys. Rev. Lett.*, **95**:081601, (2005).
16. G. P. Zeller et al. *Phys. Rev. Lett.*, **88**:091802, (2002).
17. W. M. Yao et al. *J. Phys.*, **G33**:1-1232, (2006).
18. G. Smith, In the proceedings of the PAVI11 conference, From Parity Violation to Hadronic Structure and more, *IL NUOVO CIMENTO*, **DOI: 10.1393/ncc/i2012-11297-2**, (2012)
19. R.D. Carlini et al., arXiv:1202.1255